

# Towards a Sub-percent Precision Measurement of $\sin^2 \theta_{13}$ with Reactor Antineutrinos

---

Jinnan Zhang<sup>a,b</sup> and Jun Cao<sup>a,b</sup>

<sup>a</sup>*Institute of High Energy Physics, Beijing 100049, China*

<sup>b</sup>*University of Chinese Academy of Sciences, Beijing 100049, China*

*E-mail:* [zhangjinnan@ihep.ac.cn](mailto:zhangjinnan@ihep.ac.cn), [caoj@ihep.ac.cn](mailto:caoj@ihep.ac.cn)

**ABSTRACT:** Measuring the neutrino mixing parameter  $\sin^2 \theta_{13}$  to the sub-percent precision level could be necessary in the next ten years for the precision unitary test of the PMNS matrix. In this work, we discuss the possibility of such a measurement with reactor antineutrinos. We find that a single liquid scintillator detector on a reasonable scale could achieve the goal. We propose to install a detector of  $\sim 10\%$  energy resolution at about 2.0 km from the reactors. The integrated luminosity requirement is about  $150 \text{ kton} \cdot \text{GW} \cdot \text{year}$ , corresponding to 3 years' operation of a 4 kton detector near a reactor complex of 17.4 GW thermal power like Daya Bay. Unlike the previous  $\theta_{13}$  experiments with identical near and far detectors, whose rate uncertainty is suppressed by the near-far relative measurement and the optimal baseline is at the first oscillation maximum of about 1.8 km, a single-detector measurement prefers to offset the baseline from the oscillation maximum. At low statistics  $\lesssim 10 \text{ kton} \cdot \text{GW} \cdot \text{year}$ , the rate uncertainty dominates the systematics, and the optimal baseline is about 1.3 km. At higher statistics, the spectral shape uncertainty becomes dominant, and the optimal baseline shifts to about 2.0 km. The optimal baseline keeps being  $\sim 2.0 \text{ km}$  for an integrated luminosity up to  $10^6 \text{ kton} \cdot \text{GW} \cdot \text{year}$ . Impacts of other factors on the precision  $\sin^2 \theta_{13}$  measurement are also discussed. We have assumed that the TAO experiment will improve our understanding of the spectral shape uncertainty, which gives the highest precision measurement of reactor antineutrino spectrum for neutrino energy in the range of 3–6 MeV. We find that the optimal baseline is  $\sim 2.9 \text{ km}$  with a flat input spectral shape uncertainty provided by the future summation model. The shape uncertainty would be the bottleneck of the  $\sin^2 \theta_{13}$  precision measurement. The  $\sin^2 \theta_{13}$  precision is not sensitive to the detector energy resolution and the precision of other oscillation parameters.

**KEYWORDS:** Neutrino Oscillation, Reactor Antineutrino,  $\sin^2 \theta_{13}$

---

## Contents

<b>1</b>	<b>Introduction</b>	<b>1</b>
<b>2</b>	<b>Reactor antineutrino detection and statistical analysis</b>	<b>3</b>
2.1	Reactor antineutrino spectrum prediction	3
2.2	Statistical analysis and systematics	4
<b>3</b>	<b>Sub-percent precision measurement of <math>\sin^2 \theta_{13}</math></b>	<b>7</b>
3.1	Experiment setup and precision measurement sensitivity	7
3.2	The impact of the shape uncertainty distribution	10
3.3	Systematics breakdown and sub-percent precision	11
3.4	The impact of the oscillation parameters	12
3.5	The impact of the reactor antineutrino anomaly and excess	13
3.6	The impact of the detector performance	14
<b>4</b>	<b>Conclusion</b>	<b>15</b>

---

## 1 Introduction

Since first detected in 1956 by Reines and Cowan at the Savannah River reactor, neutrinos have played an inspiring role in particle physics. Plenty of experiments prove that there are three flavors of neutrinos, and they are massive. Neutrinos are created via electroweak interactions in flavor states  $\nu_e$ ,  $\nu_\mu$ , and  $\nu_\tau$ . The neutrino oscillation phenomenon reveals that the three mass eigenstates  $\nu_{1,2,3}$  with masses  $m_{1,2,3}$  are non-degenerate from the three flavor eigenstates. The Pontecorvo-Maki-Nakagawa-Sakata (PMNS) [1, 2] matrix  $U$  is proposed to describe the mixing among massive neutrino states,  $\nu_\alpha = U_{\alpha i} \nu_i$ , where  $\alpha$  indexes flavor states and  $i$  indexes mass states. The mixing matrix can be parameterized with three mixing angles,  $\theta_{12}$ ,  $\theta_{13}$ , and  $\theta_{23}$ , plus a CP violation phase  $\delta_{\text{CP}}$ . If neutrinos are Majorana fermions, there will be two additional phases irrelevant to the neutrino oscillation. See Ref. [3] for comprehensive reviews and perspectives of neutrino physics.

Table 1 summarizes the current precision estimation of the oscillation parameters and the dominant types of experiments, taken from PDG2020 [4], as well as the projected precision in the near future. Most of them are determined with precision within a few percent except for  $\delta_{\text{CP}}$ , which is expected to be determined by the next generation neutrino experiments. The measurement of  $\sin^2 \theta_{12}$  and  $\Delta m_{21}^2$  are currently dominated by the solar neutrino experiments SNO [9] and Super-Kamiokande [10, 11], and the long-baseline reactor neutrino experiment KamLAND [12]. The accelerator and atmospheric neutrino experiments explore oscillation physics via the same oscillation channels and are sensitive to the same parameters,  $\Delta m_{32}^2/\Delta m_{31}^2$ ,  $\sin^2 \theta_{23}$ , and  $\delta_{\text{CP}}$ . The dominant measurements are

Parameter	Ordering	Value	$1\sigma$ (%)	Dominant Exps.	Prospect (% , years)
$\frac{\Delta m_{21}^2}{10^{-5} \text{ eV}^2}$	NO, IO	$7.53\pm 0.18$	2.4	Rea., Sol.	(0.3, 6) [5]
$\frac{ \Delta m_{32}^2 }{10^{-3} \text{ eV}^2}$	NO	$2.453\pm 0.034$	1.4	Acc., Atm., Rea.	(0.2, 6) [5]
	IO	$2.546\pm 0.037$	1.5		
$\sin^2 \theta_{12}$	NO, IO	$0.307\pm 0.013$	4.2	Sol., Rea.	(0.5, 6) [5]
$\frac{\sin^2 \theta_{13}}{10^{-2}}$	NO, IO	$2.18\pm 0.07$	3.2	Rea.	(2.7, - ) [6]
$\sin^2 \theta_{23}$	NO	$0.545\pm 0.021$	3.9	Acc., Atm.	(0.7–3.4, 10) [7, 8]
	IO	$0.547\pm 0.021$	3.8		
$\delta_{\text{CP}}/\pi$	NO, IO	$1.36\pm 0.17$	12.5	Acc., Atm.	TBD

**Table 1.** Current relative precision estimation of the oscillation parameters from PDG2020 [4] and the projected precision in the near future with corresponding data taking time. The  $1\sigma$  relative uncertainties and the dominant types of experiments (Exps.) are also listed. The reactor experiments (Rea.) measure  $\sin^2 \theta_{13}$  and  $\Delta m_{21}^2$  with the highest precision. The solar experiments (Sol.) contribute a lot to the  $\sin^2 \theta_{12}$  and  $\Delta m_{21}^2$  determination. The accelerator (Acc.) and atmospheric experiments (Atm.) dominate the measurements of  $\sin^2 \theta_{23}$ ,  $\Delta m_{32}^2$ , and  $\delta_{\text{CP}}$ . The estimation for both normal ordering (NO) and inverted ordering (IO) are presented.

from the NOvA [13], T2K [14], MINOS [15], Super-Kamiokande [16] and IceCube [17] experiments. The precision of the smallest mixing angle  $\sin^2 \theta_{13}$  is dominated by the reactor experiments with baselines at  $\sim \mathcal{O}(1)$  km, including the Daya Bay [6], RENO [18], and Double Chooz [19].

Towards the sub-percent precision measurements of the oscillation parameters, Table 1 also lists the prospects in the next ten years. The increasing data volume at the T2K and NOvA experiments will further improve the precision of  $\Delta m_{31}^2/\Delta m_{32}^2$  to about 1% [20, 21]. The under-construction medium baseline reactor neutrino experiment JUNO will start operation in 2023 and can measure  $\sin^2 \theta_{12}$ ,  $\Delta m_{21}^2$ , and  $\Delta m_{31}^2/\Delta m_{32}^2$  to the sub-percent precision level within one year [5, 22]. The next-generation experiments DUNE [7] and Hyper-Kamiokande [8] are designed to determine the CP-violation phase  $\delta_{\text{CP}}$ , the octant of  $\sin^2 \theta_{23}$ , and the mass ordering. After ten years of data taking, they can measure  $\sin^2 \theta_{23}$  to the precision from sub-percent to  $\sim 3.4\%$ , depending on the true octant. Hyper-Kamiokande and DUNE will also measure  $\Delta m_{32}^2/\Delta m_{31}^2$  to the sub-percent precision level with channels other than JUNO. The DUNE measurement of  $\sin^2 \theta_{13}$  can also approach the precision of Daya Bay with high exposure [7]. In the next ten years, we can expect sub-percent precision measurements for most oscillation parameters,  $\sin^2 \theta_{12}$ ,  $\sin^2 \theta_{23}$ ,  $\Delta m_{21}^2$ , and  $\Delta m_{32}^2/\Delta m_{31}^2$ . However, for  $\sin^2 \theta_{13}$ , there is no more plan for more precise measurement. The Daya Bay experiment has been shut down in 2020. The precision of  $\sin^2 \theta_{13}$  with the full dataset of neutron-capture on Gadolinium is expected to be about 2.7%. It would be vital for the PMNS matrix’s sub-percent precision unitary test to measure  $\sin^2 \theta_{13}$  to a sub-percent level.

In this work, we discuss the possibility of measuring  $\sin^2 \theta_{13}$  to the sub-percent precision level with reactor antineutrinos via the Inverse Beta Decay (IBD) interaction. The electron antineutrinos ( $\bar{\nu}_e$ ) from nuclear reactors are a very powerful source for measuring the  $\theta_{13}$  mixing angle. We could get large statistics and predict the energy spectrum precisely. This paper is organized as follows. We present the survival probability calculation for  $\bar{\nu}_e$ , the observed spectrum prediction, and analysis strategy in Sec. 2. In Sec. 3, the numerical results show that, by installing a single 4 kton detector of  $\sim 10\%$  energy resolution at the baseline of  $\sim 2.0$  km from a reactor complex like Daya Bay, the experiment could measure  $\sin^2 \theta_{13}$  to the sub-percent precision level within about 3 years. We also study the impact of different factors that may increase or decrease the sensitivity in that section. Finally, the summary and conclusions are posted in Sec. 4.

## 2 Reactor antineutrino detection and statistical analysis

The IBD interaction,  $\bar{\nu}_e + p \rightarrow n + e^+$ , is the typical channel to detect the  $\bar{\nu}_e$  in the few-MeV range with liquid scintillator (LS) detectors for its large cross-section. In this reaction, the electron antineutrino interacts with a proton ( $p$ ) in the LS, creating a positron ( $e^+$ ) and a neutron ( $n$ ). The  $e^+$  takes most energy of the original neutrino and quickly deposits its energy and annihilates into gammas, giving a prompt signal. Thus, the experiment can extract neutrino oscillation parameters by looking at the observed positron energy spectrum. While the neutron is thermalized in the detector and captured by a nucleus, it produces a delayed signal. The time, space, and energy correlation between the prompt and delayed signals are powerful to suppress the backgrounds. This section presents the approach to predicting the visible energy spectrum of the reactor antineutrinos with IBD reaction. Then we introduce the statistical method to calculate the  $\sin^2 \theta_{13}$  sensitivity. We also carefully estimate the systematic uncertainties based on the experiences of previous and current experiments.

### 2.1 Reactor antineutrino spectrum prediction

The commercial nuclear power plants are “free” and powerful artificial  $\bar{\nu}_e$  source for measuring  $\sin^2 \theta_{13}$ , which generate electron antineutrinos via subsequent  $\beta$  decays of the fission products of mainly four isotopes,  $^{235}\text{U}$ ,  $^{238}\text{U}$ ,  $^{239}\text{Pu}$ , and  $^{241}\text{Pu}$ . After creation, the  $\bar{\nu}_e$  propagates in mass eigenstates on the way to the detector and then is detected with the weak eigenstate  $\bar{\nu}_e$ . Under the assumption of three flavor mixing, the survival probability  $\mathcal{P}(\bar{\nu}_e \rightarrow \bar{\nu}_e)$  can be expressed as,

$$\begin{aligned} \mathcal{P}(\bar{\nu}_e \rightarrow \bar{\nu}_e) = & 1 - \sin^2 2\theta_{13}(\cos^2 \theta_{12} \sin^2 \Delta_{31} + \sin^2 \theta_{12} \sin^2 \Delta_{32}) \\ & - \cos^4 \theta_{13} \sin^2 2\theta_{12} \sin^2 \Delta_{21}, \end{aligned} \quad (2.1)$$

where  $\Delta_{ji} = \Delta m_{ji}^2 L / (4E_{\bar{\nu}})$ ,  $L$  is the baseline and  $E_{\bar{\nu}}$  is electron antineutrino energy. The terrestrial matter effects can influence the oscillation pattern [23, 24]. For a several-kilometer baseline experiment, the matter effects are relatively small. Nonetheless, we include the matter effects in this work [25, 26] with a typical constant matter density

$\rho = 2.6 \text{ g/cm}^3$ . The matter effects may distort the survival probability up to relatively 0.2% with negligible uncertainty.

The visible prompt energy ( $E_{\text{prompt}}$ ) spectrum from reactor  $r$  at detector  $d$  at time  $t$  can be predicted as,

$$S_{d,r}(E_{\text{prompt}}, t) = \left( \epsilon_d \cdot N_{p,d} \int dE_{\bar{\nu}_e} \frac{\mathcal{P}_{ee}(E_{\bar{\nu}_e}, L_{dr})}{4\pi L_{dr}^2} \frac{W_r(t)}{\sum_i f_{ir}(t) e_i} \sum_i f_{ir}(t) \phi_i(E_{\bar{\nu}_e}) \sigma_{\text{tot}}(E_{\bar{\nu}_e}) \right) \otimes G(E_{e^+}, \sigma_d), \quad (2.2)$$

where  $\epsilon_d$  and  $N_{p,d}$  are the detection efficiency and number of target protons of detector  $d$ , respectively. A 12% hydrogen fraction from the Daya Bay experiment [27] is used to calculate the number of target protons with corresponding target mass.  $\mathcal{P}_{ee}(E_{\bar{\nu}_e}, L_{dr})$  is the  $\bar{\nu}_e$  survival probability with energy  $E_{\bar{\nu}_e}$  and baseline  $L_{dr}$  is the distance from detector  $d$  to reactor  $r$ .  $W_r(t)$  and  $f_{ir}(t)$  are the thermal power and fission fraction of the reactor  $r$  at time  $t$ . The nuclear reactors release energy by fission reactions, and  $e_i$  and  $\phi_i(E_{\bar{\nu}_e})$  are the energy yield and neutrino spectrum per fission of isotope  $i$ , respectively. In this work, we set the average fission fraction to be 0.564, 0.076, 0.304, and 0.056 [28] with the mean energy per fission of 202.36 MeV, 205.99 MeV, 211.12 MeV, and 214.26 MeV [29, 30] for  $^{235}\text{U}$ ,  $^{238}\text{U}$ ,  $^{239}\text{Pu}$ , and  $^{241}\text{Pu}$ , respectively. The Huber-Mueller model ( $^{235}\text{U}$ ,  $^{239}\text{Pu}$ , and  $^{241}\text{Pu}$  from Ref. [31],  $^{238}\text{U}$  from Ref. [32]) is a widely used model for calculating the  $\bar{\nu}_e$  energy spectrum of the isotopes. The measurements from the Daya Bay [33], Double Chooz [19], and RENO [34] experiments reveal that both the measured neutrino flux and shape are inconsistent with the Huber-Mueller model. Nevertheless, We find that the measured antineutrino flux and spectrum from the Daya Bay experiment [28] and the Huber-Mueller flux model give consistent  $\sin^2 \theta_{13}$  sensitivities, which is discussed in detail in Sec. 3.5. For simplicity and without losing accuracy, we employ the Huber-Mueller flux model here.

The total cross-section of the IBD reaction  $\sigma_{\text{tot}}(E_{\bar{\nu}})$  can be precisely calculated [35, 36]. The term “ $\otimes G(E_{e^+}, \sigma_d)$ ” represents the Gaussian smearing processes to take into account the energy resolution of detector  $d$  with resolution  $\sigma_d$ . The energy resolution is not a key factor for  $\sin^2 \theta_{13}$  measurement at several kilometers. Thus, we set the energy resolution of the detector to be  $10\%/\sqrt{E(\text{MeV})}$ . A detector with such resolution would be sufficiently sensitive to  $\sin^2 \theta_{13}$  and not too expensive. Nonetheless, we study the impact of the energy resolution in Sec. 3.6. Given the prompt energy interval  $[E_{\text{prompt},k}, E_{\text{prompt},k+1}]$ , we can calculate the expected number of signals  $T_{d,k}$  as,

$$T_{d,k} = \int_{E_{\text{prompt},k}}^{E_{\text{prompt},k+1}} dE_{\text{prompt}} \int_{t_{\text{DAQ}}} dt \sum_r S_{d,r}(E_{\text{prompt}}, t), \quad (2.3)$$

where  $t_{\text{DAQ}}$  is the total data taking time.

## 2.2 Statistical analysis and systematics

To extract the  $\sin^2 \theta_{13}$  sensitivity of the experiment, we firstly generate a binned Asimov dataset with the nominal setup and approach described above. Then we fit the pseudo data

with hypotheses using the Poisson-likelihood  $\chi^2$  with nuisance parameters and pull terms to account for the systematic uncertainties [37],

$$\chi^2 \equiv 2 \sum_{d,k} \left( T_{d,k}(\boldsymbol{\theta}, \boldsymbol{\epsilon}) - D_{d,k} + D_{d,k} \ln \frac{D_{d,k}}{T_{d,k}(\boldsymbol{\theta}, \boldsymbol{\epsilon})} \right) + \sum_{s,d,k} \left( \frac{\epsilon_{s,d,k}}{\sigma_{s,d,k}} \right)^2, \quad (2.4)$$

where  $D_{d,k}$  is the event rate in the  $k$ -th energy bin of detector  $d$ .  $T_{d,k}$  is the theoretically predicted value with the oscillation parameters  $\boldsymbol{\theta}$  and the nuisance parameters  $\boldsymbol{\epsilon}$ .  $\sigma_{s,d,k}$  in the pull term represents the estimation of the  $s$ -th systematic uncertainties for the  $k$ -th energy bin of detector  $d$ , and  $\epsilon_{s,d,k}$  is the corresponding nuisance parameter. In this work, we perform the binned analysis using 320 equal bins for prompt energy from 0.8 MeV to 12 MeV.

The systematic uncertainties are especially important for the precision measurement of  $\sin^2 \theta_{13}$  with large statistics. Based on the experiences and prospects of reactor experiments Daya Bay [6, 38, 39], Double Chooz [40], RENO [18], KamLAND [41], and JUNO [22], here we list the estimation of the systematic uncertainties used in this work in Table 2.

Rate	Uncertainty (%)	Shape	Uncertainty (%)
Flux prediction	2.0 [19, 33, 34]	Flux prediction	<1.0 (2–5 MeV) [42]
Fission fraction	0.6 [19, 34, 38]	Background subtraction	0.1
Thermal power	0.5 [19, 34, 38]	Total	With TAO, $\sim 1.0$
Proton number	0.9 [38]		
IBD selection	1.0	Energy calibration	0.5 [39]
Total	$\sim 3.0$		

**Table 2.** Summary of major systematic uncertainties and their values used in this work. The spectral shape uncertainties are estimated for the bin width of 35 keV.

We pack the systematics into several groups: rate uncertainty, spectral shape uncertainty, and energy calibration uncertainty. We estimate their values and assess their impact on  $\sin^2 \theta_{13}$  precision measurement sensitivity as follows.

1. The overall event rate systematic uncertainty contains all the effects that may affect the normalization of the total event number. We set the value to be 3% as the quadratic sum of all independent sources. In Eq. (2.4), we assign a nuisance parameter  $\epsilon_{\text{rate}}$  with constraint  $\sigma_{\text{rate}}$  to take into account this uncertainty. The major source of the rate uncertainty is the predicted number of antineutrinos yielded by the nuclear reactor. The model prediction uncertainty can be constrained by the absolute reactor neutrino flux measurement by the near detectors of the Daya Bay [33], Double Chooz [19], and RENO [34] experiments, which include the uncertainty of the IBD cross-section, and the overall uncertainty is less than 2%. We also include the rate uncertainties per reactor from the fission fraction (0.6% in total) and thermal power (0.5%) [19, 34, 38]. On the detection side, we assume that the uncertainty of

the number of target protons would be 0.9% and that of the IBD selection efficiency would be at the 1% level, taken from the Daya Bay experiment [38].

2. The spectral shape uncertainty refers to the factors that may distort the spectral shape and are uncorrelated from bin to bin. It is essential for high precision measurement. The reactor antineutrino flux prediction based on current knowledge from experiments and theoretical models has a relatively larger uncertainty from 2% [19, 28, 34] to more than 5% [31, 32, 43, 44]. In this work, we set the reactor antineutrino spectral shape uncertainty constrained by the future short-baseline experiment, which is <1% for a bin width of about 35 keV in most signal energy range (2–5 MeV). In Eq. (2.4), we assign each energy bin a nuisance parameter  $\epsilon_{\text{shape},k}$  with constraint  $\sigma_{\text{shape},k}$  to take into account this uncertainty. The Taishan Antineutrino Observatory (TAO) [42], with a ton-level Gadolinium-doped Liquid Scintillator (GdLS) detector at a baseline of 30 m from a reactor core of the Taishan Nuclear Power Plant, will start operation in 2023 as a satellite experiment of the JUNO experiment. Thanks to the almost full optical coverage with high photon detection efficiency (>50%) Silicon Photomultipliers (SiPMs), the TAO energy resolution is better than 2% at 1 MeV. After six years of data taking, TAO could measure the reactor spectral shape to the precision of better than 1% in the prompt energy range of 2–5 MeV, with the bin width of about 35 keV to investigate the possible fine structure in the spectrum. The reactor  $\bar{\nu}_e$  flux shape constrained by the direct measurement of the TAO experiment is more precise than the current summation (or ab-initio) [43, 44] or the conversion [31, 32] methods; and the shape uncertainty distribution is dominated by the statistics. Differently, the relative shape uncertainty distribution of the summation or conversion model prediction is approximately flat in most of the energy range. We find that the relative shape uncertainty distribution has a large impact on the high precision  $\sin^2 \theta_{13}$  measurement, and more details are described in Sec. 3.2. The antineutrinos from the spent nuclear fuel (0.3%) and non-equilibrium (0.6%) are also taken into account with 30% relative rate uncertainty [6, 45]. The background subtraction may also induce spectral shape uncertainty. We do not include the specific background in this work; instead, we assess their impacts within the total spectral shape uncertainty. It is reasonable for a detector with a baseline of several kilometers to get enough shield to suppress the cosmogenic backgrounds. We also assume that with the technology similar to JUNO [46], the radioactive background would be sufficiently small. We calculate the reactor antineutrino event rate and roughly estimate the rate of the possible backgrounds after the IBD selection with similar criteria as the KamLAND experiment [12]. We find that the relative spectrum uncertainty from the background subtraction should be at the level of 0.1%. The backgrounds considered in the estimations are radioactive background [46], cosmogenic background [47], Geo-neutrino and atmospheric neutrinos [48]. The spectral shape uncertainty provided by the TAO experiment has taken into account the uncertainty of the energy nonlinearity. We also assume the nonlinearity uncertainty of our future experiment is most correlated to the TAO experiment. The residual nonlinearity and its uncertainty are ignored.

3. The absolute energy scale uncertainty can be controlled by proper calibration strategy, as verified by the Daya Bay experiment [39]. This work assumes the absolute energy scale calibration uncertainty to be 0.5%. To account for this uncertainty, we assign a nuisance parameter  $\epsilon_{\text{calib}}$  with constraint  $\sigma_{\text{calib}}$ . In predicting the observed energy spectrum of Eq. (2.2), we analytically replace the expected energy  $E_0$  by  $(1+\epsilon_{\text{calib}})\cdot E_0$ , on which the energy resolution is defined.

To extract the sensitivity of  $\sin^2\theta_{13}$ , we minimize the  $\chi^2$  defined in Eq. (2.4) with respect to all the oscillation parameters and nuisance parameters. For the oscillation parameters, we use the prior central values and uncertainties in Table 1 from PDG2020 [4] to constrain  $\sin^2\theta_{12}$ ,  $\Delta m_{21}^2$ , and  $\Delta m_{31}^2$ . The  $\sin^2\theta_{13}$  sensitivity weakly depends on these parameters, as shown in Sec. 3.4. To find the best location and luminosity requirements of the experiment, we defined the  $1\sigma$  precision sensitivity of  $\sin^2\theta_{13}$  as

$$P_{1\sigma} = \frac{(x^{\text{up}} - x^{\text{low}})}{2 \cdot x_{\text{bft}}}, \quad (2.5)$$

where  $x^{\text{up}}(x^{\text{low}})$  is the upper (lower) bound for parameter  $x$  (i.e.,  $\sin^2\theta_{13}$ ) at  $1\sigma$  level, i.e., at which the marginalized  $\Delta\chi^2(x)$  ( $\equiv \chi^2(x) - \chi_{\text{min}}^2$ ) is equal to 1.  $x_{\text{bft}}$  is the best fit value of the parameter.

### 3 Sub-percent precision measurement of $\sin^2\theta_{13}$

The reactor antineutrino experiments can measure  $\sin^2\theta_{13}$  by installing identical near and far detectors, like the Daya Bay [49], RENO [18], and Double Chooz [19] experiments. The identical detectors could tremendously reduce the rate systematic uncertainties with the near-far relative measurement. However, as the statistics increase, the spectral shape systematic uncertainty becomes more important, which is hard to be suppressed by the near-far detector strategy. Moreover, building a kton-level detector at a very short baseline is not feasible with no vision of the oscillation effect. It is much more attractive and has more physics potential to allocate the resources from digging two underground experiment halls to building a larger far detector. Thus, we propose an experiment to build a single detector several kilometers from the reactor. With the spectrum prediction and systematic uncertainty estimation in Sec. 2, we numerically calculate the precision of  $\sin^2\theta_{13}$  to find the best choice of the baseline. Then, we propose the nominal setup and discuss the impact of various factors on the sensitivity.

#### 3.1 Experiment setup and precision measurement sensitivity

In this work, we quote the  $\sin^2\theta_{13}$  precision measurement sensitivity for different statistics using the integrated luminosity [kton · GW · year] under the assumption of a single reactor. Take the Daya Bay experiment [49] as an example. The reactor's thermal power is 17.4 GW. The total target mass of the four far detectors is 80 tons. Thus, the total integrated luminosity is about 12.5 kton · GW · year from the start of data taking in 2011 to the shutdown in 2020.



Fig. 1 shows the unoscillated measurable antineutrino energy spectrum (flux multiplied by the total IBD cross-section) at 1 km, the relative spectral shape uncertainty constrained by the future TAO experiment [42], together with the  $\bar{\nu}_e$  disappearance probability at different baselines. The  $\bar{\nu}_e \rightarrow \bar{\nu}_e$  disappearance amplitude represents the oscillation parameter

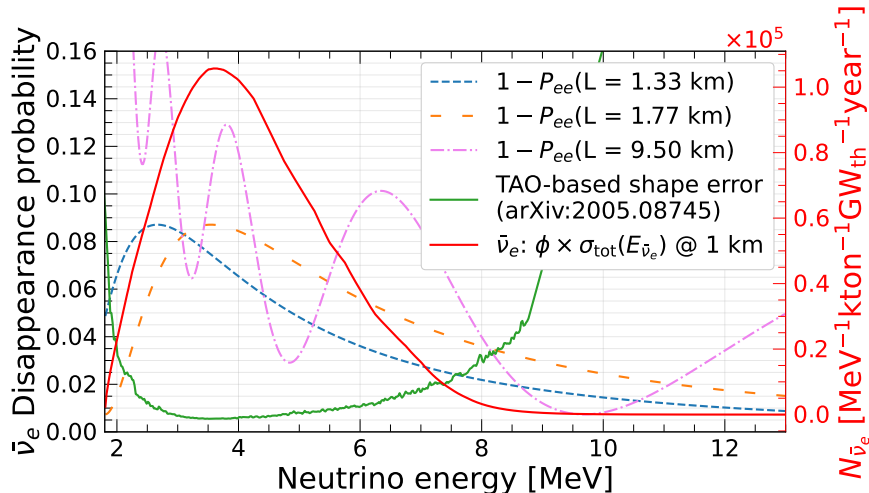


**Figure 1.** The unoscillated measurable reactor antineutrino energy spectrum  $\phi \times \sigma_{\text{tot}}(E_{\bar{\nu}_e})$  (flux multiplied by the total IBD cross-section) at 1 km and the  $\bar{\nu}_e$  disappearance probability  $P_{ee}$  at different baselines. For a single detector, the rate uncertainty would mimic the oscillation pattern of  $\sin^2 \theta_{13}/\Delta m_{31}^2$  when the oscillation maximum is at the peak of the antineutrino spectrum. The relative spectral shape uncertainty constrained by the TAO experiment (green line) [42] shows that the most precise neutrino energy region is 3–6 MeV.

$\sin^2 \theta_{13}$ ; thus,  $\sin^2 \theta_{13}$ 's high precision measurement requires low uncertainties around the disappearance probability peak energy. The green line in the figure shows that the direct measurement can constrain the shape uncertainty to a sub-percent level for the neutrino energy of 3–6 MeV [42]. Due to the limit of statistics, however, the relative uncertainties are large at the low and high energy end. Thus, as discussed in Sec. 2.2, if the summation model could predict the reactor antineutrino flux to be consistent with the measurement of the TAO experiment, the spectral shape uncertainty of their combined prediction would be better than 1%. Therefore, hereafter we set a 1% spectral shape relative uncertainty to study the optimal baseline of a future  $\sin^2 \theta_{13}$  measurement experiment.

With a 1% spectral shape uncertainty, Fig. 2 shows the  $1\sigma$  contour of the precision measurement sensitivity on  $\sin^2 \theta_{13}$  for different baselines and integrated luminosities. The optimal baseline for the most efficient  $\sin^2 \theta_{13}$  precision measurement varies with the increase of the integrated luminosity. The top pad of Fig. 2 shows the optimal baseline is about 1.3 km for low statistics  $\lesssim 60$  kton  $\cdot$  GW  $\cdot$  year and gradually shifts to about 2.9 km as statistics increases. At  $\sim 2.9$  km, the experiment could measure  $\sin^2 \theta_{13}$  to a precision of sub-percent level with a  $\sim 10^3$  kton  $\cdot$  GW  $\cdot$  year luminosity. Besides, we find that the precision is limited to  $\sim 1\%$  level by the spectral shape uncertainty, as the sensitivity will not be better with the increase of luminosity after  $\sim 10^4$  kton  $\cdot$  GW  $\cdot$  year. With such

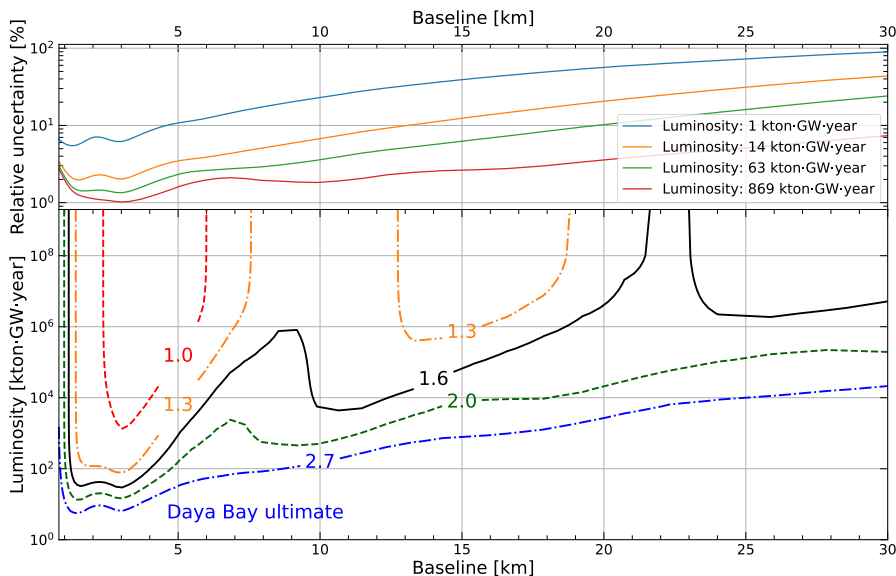


**Figure 2.** The  $1\sigma$  contour of the precision measurement sensitivity on  $\sin^2 \theta_{13}$  for different baselines and integrated luminosities. The top pad shows the sensitivity as a function of baselines for luminosities of 1, 14, 63, and 869 kton·GW·year. The optimal baseline shifts from  $\sim 1.3$  km at low statistics to  $\sim 2.9$  km at high statistics. The bottom pad shows the required luminosity to reach given precision, from 2.7% to 1.0% labelled on the curves, at different baselines. The spectral shape uncertainty is set to be 1% for a bin width of 35 keV.

spectral shape uncertainty, the single detector at the first oscillation maximum of  $\sim 1.8$  km would be impossible to measure  $\sin^2 \theta_{13}$  to the precision of a sub-percent level.

The baseline preference differs from those reactor experiments with identical near and far detectors [50], whose optimal baseline at about 1.8 km, the first oscillation maximum for reactor antineutrinos. The major difference is that the relative rate uncertainty is suppressed from  $\sim 3\%$  for a single detector measurement to  $\sim 0.1\%$  for the identical near and far detector configuration. The oscillation parameter  $\sin^2 \theta_{13}$  characterizes the disappearance amplitude, which can be mimicked by the rate uncertainty nuisance parameter when the disappearance maximum is at the same energy as the measurable reactor antineutrino energy spectrum. The offset of the oscillation maximum and unoscillated measurable antineutrino energy spectrum is shown in Fig. 1; the absolute rate uncertainty is important for a single detector at low statistics.

As the statistics increases, the spectral shape distortion contributes more and more sensitivity since each energy bin has enough statistics to reflect the oscillation effect, and all bins share the same absolute rate uncertainty. The correlation among different bins thus suppresses the impact of the rate uncertainty at high statistics. Shifting the baseline from the rate oscillation maximum will help further reduce the impact of the rate uncertainty by offsetting the oscillation maximum energy bin from the peak of the reactor neutrino spectrum. At larger baselines, there are more oscillation cycles in the measured spectrum; thus, the error cancellation due to correlation among different bins is enhanced. Further-

more, multiple cycle measurement helps to reduce the energy correlated uncertainties. The optimal baseline comes from the balance of systematic uncertainty suppression and the statistics loss.

With spectral shape uncertainty given by the future summation model, the optimal baseline keeps being  $\sim 2.9$  km. We find that the 1% shape uncertainty became dominant for the luminosity larger than  $20 \text{ kton} \cdot \text{GW} \cdot \text{year}$ . To verify the impact of the spectral shape uncertainty, here, we numerically calculate the sensitivity as a function of shape uncertainty for an experiment with the luminosity of  $10^4 \text{ kton} \cdot \text{GW} \cdot \text{year}$  at 2.9 km. Fig. 3 shows the  $\sin^2 \theta_{13}$  precision measurement sensitivity for different input shape uncertainties. It is shown that the shape uncertainties is the bottleneck of the high precision measurement of  $\sin^2 \theta_{13}$ .

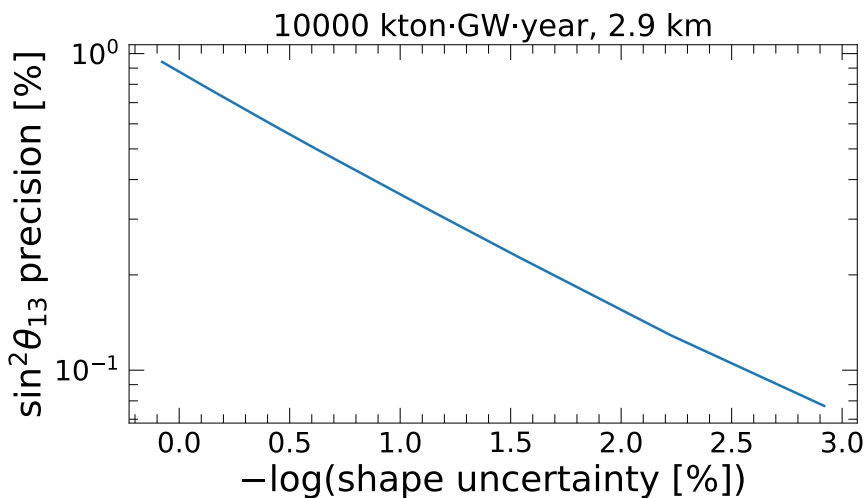


**Figure 3.** The  $\sin^2 \theta_{13}$  precision sensitivity as a function of the input spectral shape uncertainty. The x-axis is  $-\log(\sigma_{\text{shape}})$ , where  $\sigma_{\text{shape}}$  is spectral relative shape uncertainty in %. The baseline is 2.9 km and the luminosity is  $10^4 \text{ kton} \cdot \text{GW} \cdot \text{year}$ .

### 3.2 The impact of the shape uncertainty distribution

At large luminosity, the dominant uncertainty is the spectral shape uncertainty; thus, the optimal baseline highly depends on the energy distribution of the shape uncertainty. In the above discussion, we use a 1% spectral relative shape uncertainty. In the near future, after the TAO experiment starts running, we can use the direct measurement of the reactor  $\bar{\nu}_e$  to constrain the spectral shape uncertainty. The baseline preference will be different with such a spectral shape uncertainty setup. Fig. 4 shows the  $1\sigma$  contour of the precision measurement sensitivity on  $\sin^2 \theta_{13}$  using the TAO measurement as an external spectral shape uncertainty constraint. It is shown that the optimal baseline is about 1.3 km for low statistics  $\lesssim 10 \text{ kton} \cdot \text{GW} \cdot \text{year}$  and shifts to about 2.0 km as statistics increase. With the luminosity of  $\sim 150 \text{ kton} \cdot \text{GW} \cdot \text{year}$ , the experiment could measure  $\sin^2 \theta_{13}$  to a precision of sub-percent level.

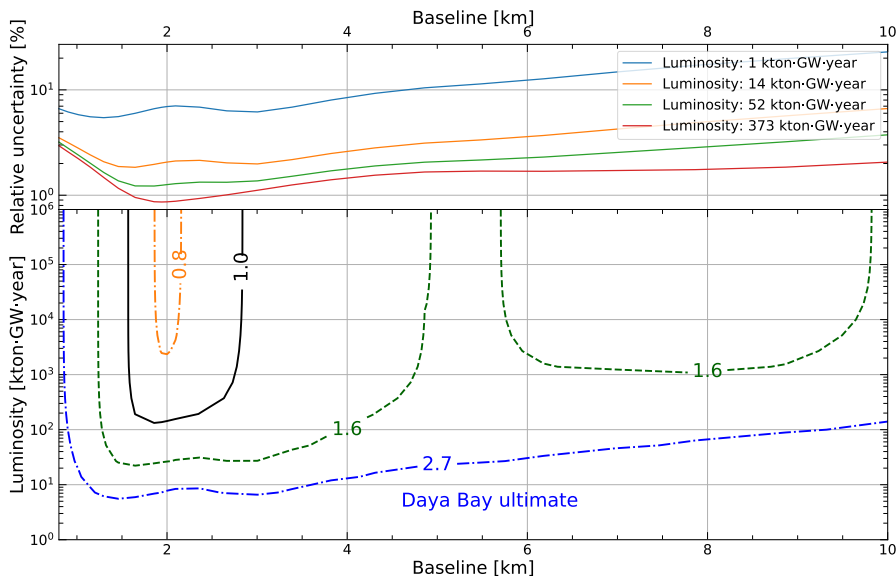


**Figure 4.** The  $1\sigma$  contour of the precision measurement sensitivity on  $\sin^2 \theta_{13}$  for different baselines and integrated luminosities. The top pad shows the sensitivity as a function of baselines for luminosities of 1, 14, 52, and 373 kton·GW·year.. The optimal baseline shifts from  $\sim 1.3$  km at low statistics to  $\sim 2.0$  km at high statistics. The bottom pad shows the required luminosity to reach 0.8% (dash-dotted orange line), 1.0% (black line), 1.6% (dash green line), and 2.7% (dash-dotted blue line) precision at different baselines. The spectral shape uncertainty is constrained by the TAO experiment.

With TAO-based spectral shape uncertainty, the required luminosity to reach 1% precision is less than that with the flat 1% assumption. The reason is that the TAO-based uncertainty is better than 1% for  $E_\nu \in (3, 6)$  MeV, which is the peak of unoscillated reactor antineutrino and thus has the largest statistics.

### 3.3 Systematics breakdown and sub-percent precision

Based on Fig. 2 and Fig. 4, the most efficient baseline for sub-percent measurement of  $\sin^2 \theta_{13}$  is about 2.0 km. Thus, we set the nominal baseline to be 2.0 km and study the impact of different systematic uncertainties. Fig. 5 shows the breakdown of the statistical and systematic uncertainties for the precision measurement sensitivity of  $\sin^2 \theta_{13}$  at different luminosities. It helps us to identify the most important systematic uncertainties at different luminosities. The rate uncertainty would be the dominant systematics at low luminosity  $\lesssim 60$  kton·GW·year; then, the shape uncertainty would be dominant. The impact of energy scale calibration uncertainty is negligible at low statistics and would have a minor impact as luminosity increases. The shape uncertainty would totally dominate the  $\sin^2 \theta_{13}$  precision measurement with luminosity larger than  $\sim 10^3$  kton·GW·year.

With the integrated luminosity of about 150 kton·GW·year, the experiment can measure  $\sin^2 \theta_{13}$  to the sub-percent level precision. One feasible design is to install a 10% energy resolution, 4 kton liquid scintillator detector near a reactor complex like Daya Bay,

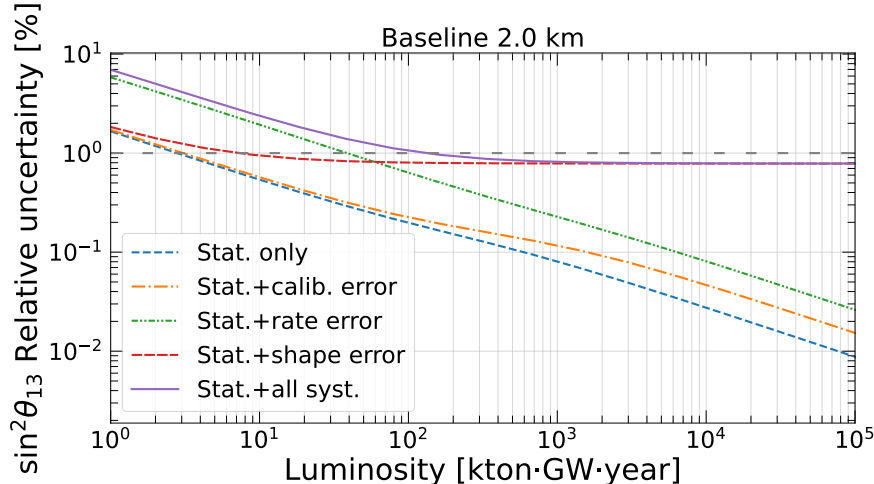


**Figure 5.** The  $\sin^2 \theta_{13}$  precision measurement sensitivity under different consideration of the systematic uncertainties as a function of integrated luminosity. With the integrated luminosity larger than  $\sim 60$  kton  $\cdot$  GW  $\cdot$  year, the shape uncertainty gradually dominates the precision measurement of  $\sin^2 \theta_{13}$ .

whose thermal power is about 17.4 GW. With such a setup, consider a typical  $> 80\%$  signal selection efficiency and 11/12 reactor duty cycle [38], the experiment could measure  $\sin^2 \theta_{13}$  to the sub-percent precision level within three years.

### 3.4 The impact of the oscillation parameters

The optimal baseline ( $\sim 2.0$  km) we propose in this work depends on the central values of the oscillation parameters and the energy spectrum of the reactor antineutrino. Thus, we generate several Asimov data sets with different oscillation parameter values and mass orderings to assess the impact. The results using the nominal luminosity 150 kton  $\cdot$  GW  $\cdot$  year is shown in Fig. 6, where we always update  $\Delta m_{32}^2$  correspondingly assuming  $\Delta m_{32}^2 = \Delta m_{31}^2 - \Delta m_{21}^2$ .

It can be seen that the  $\sin^2 \theta_{13}$  measurement is almost independent of the true values of the solar oscillation parameters  $\sin^2 \theta_{12}$  and  $\Delta m_{21}^2$  at such baseline. The sensitivity weakly depends on the true value of  $\Delta m_{31}^2$ . The relative precision sensitivity is, as we expected, almost inversely linear proportional to the true value of  $\sin^2 \theta_{13}$ . This dependence shows that the ability of the detector to locate the absolute value of  $\sin^2 \theta_{13}$  is robust.

The true value of  $\sin^2 \theta_{13}$  is important for the sub-percent relative precision measurement of  $\sin^2 \theta_{13}$ ; if the true value is smaller, the detector will have to take more data for the sub-percent precision measurement. The central value estimated by PDG2020 [4] is 0.0218, and recently the results from global fit groups yield that the central value is 0.0223 ( $\sim 2\%$  larger) [51–53]. With a larger true value, the experiment can measure  $\sin^2 \theta_{13}$  to the sub-percent precision level with fewer statistics.

In Sec. 2.2, we constrain  $\sin^2 \theta_{12}$ ,  $\Delta m_{21}^2$ , and  $\Delta m_{31}^2$  using the PDG2020 central values

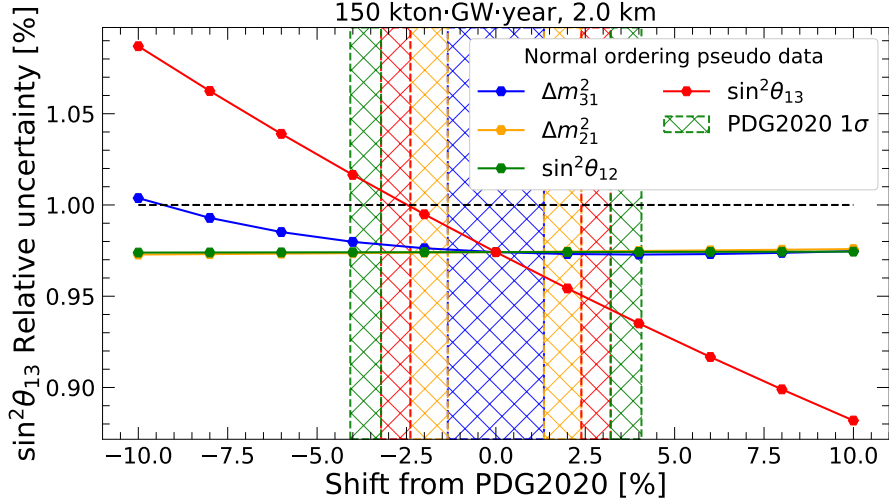


**Figure 6.** The  $\sin^2 \theta_{13}$  precision measurement sensitivity for the Asimov pseudo data generated with the oscillation parameters shifted from PDG2020 [4]. The green and orange lines are on the top of each other since the roles of  $\sin^2 \theta_{12}$  and  $\Delta m_{21}^2$  true values are almost the same for the  $\sin^2 \theta_{13}$  measurement. The shadow area represents the  $1\sigma$  region given in PDG2020. The normal and inverted ordering hypotheses yield almost the same results.

and  $1\sigma$  uncertainties by adding a pull term defined in Eq. (3.1),

$$\chi_{\text{pull}}^2 \equiv \sum_{\theta} \frac{(\theta - \theta_0)^2}{\sigma_{\theta}^2}, \quad (3.1)$$

where  $\theta$  refers to the oscillation parameters, including  $\sin^2 \theta_{12}$ ,  $\Delta m_{21}^2$ , and  $\Delta m_{31}^2$ .  $\theta_0$  and  $\sigma_{\theta}$  are the central values and  $1\sigma$  uncertainties. With the nominal setup, we find that the  $\sin^2 \theta_{13}$  precision sensitivity keeps almost unchanged (relative difference within 0.2%) whether we constrain, fix, or free  $\Delta m_{31}^2$ . Actually, the experiment can also measure  $\Delta m_{31}^2$  to the precision of  $\sim 0.6\%$  with  $150 \text{ kton} \cdot \text{GW} \cdot \text{year}$  luminosity. As a future experiment, we can anticipate the future external information of the oscillation parameters. With the  $\sin^2 \theta_{12}$ ,  $\Delta m_{21}^2$ , and  $\Delta m_{31}^2$  constraints from the projected relative precision listed in Table 1, the  $\sin^2 \theta_{13}$  precision sensitivities would be relatively  $\sim 0.5\%$  better. When we fix all other oscillation parameters,  $\sin^2 \theta_{12}$ ,  $\Delta m_{21}^2$ , and  $\Delta m_{31}^2$ , the  $\sin^2 \theta_{13}$  precision sensitivity would be relatively  $\sim 0.1\%$  better than the projected relative precision. The experiment can measure  $\sin^2 \theta_{13}$  to the sub-percent precision level with other oscillation parameters fixed or constrained with external information. However, since this detector is not designed for  $\sin^2 \theta_{12}$  and  $\Delta m_{21}^2$  measurements, when we free all other oscillation parameters, the nominal sensitivity reduces from 1% to  $\sim 2.6\%$ . Thus, for a  $\sin^2 \theta_{13}$  high precision measurement experiment, using external information could help accomplish the major physics goal.

### 3.5 The impact of the reactor antineutrino anomaly and excess

As shown in Fig. 1, the offset of the optimal baseline depends on the unoscillated measurable reactor  $\bar{\nu}_e$  energy spectrum. In Sec. 2.1, we use the Huber-Mueller model [31, 32]

as the nominal flux model to predict the observed reactor antineutrino energy spectrum. However, a  $\sim 6\%$  absolute flux deficit compared to the Huber-Mueller model is found by the measurements of the Daya Bay [33], Double Chooz [19], and RENO [34] experiments. This deficit is the so-called reactor antineutrino anomaly. Besides, the experiments also find an excess around 5 MeV on the spectral shape called “5 MeV excess” [3].

We can use the flux measured by previous reactor neutrino experiments to explore the impact of reactor antineutrino anomaly and excess. This work employs the unfolded isotope flux from the Daya Bay experiment given in Ref. [28], which naturally includes both effects. In the interest of study the flux model dependence of the sensitivity, we switch the flux calculation of all isotopes in Eq. (2.2) from  $\sum_i f_i \phi_i(E_{\bar{\nu}})$  to Eq. (8) of Ref. [28]. With all the other setups, including systematics, same as in Sec. 2, Table 3 gives the  $1\sigma$  precision sensitivity of  $\sin^2 \theta_{13}$  with different isotope flux models.

$\sin^2 \theta_{13}$ $1\sigma$ uncertainty (%)	Huber+Mueller [31, 32]	Daya Bay unfolded [28]
Stat.	0.170	0.173
Stat.+rate error	0.524	0.535
Stat.+calib. error	0.198	0.200
Stat.+shape error	0.796	0.797
Stat.+all syst.	0.974	0.977

**Table 3.** The  $\sin^2 \theta_{13}$   $1\sigma$  precision sensitivity under different consideration of the uncertainties with the Huber-Mueller flux model and the Daya Bay unfolded flux model. The latter naturally includes the reactor antineutrino anomaly and the “5 MeV excess”. The 6% deficit reduces the statistics and the “5 MeV excess” benefits the  $\sin^2 \theta_{13}$  precision measurement relatively by  $\sim 0.3\%$ . All results are for the detector installed at 2.0 km from the reactor and 150 kton · GW · year luminosity.

It can be seen that the reactor antineutrino anomaly and “5 MeV” excess have a minor impact on the sub-percent precision measurement of  $\sin^2 \theta_{13}$ . The latter effect means there are more events at the neutrino energy around 6 MeV, which helps the measurement by providing more statistics at this energy. As shown in Fig. 1, more statistics around 6 MeV slightly improve the sensitivity as shown in Table 3. With the existing measurements and the coming high precision measurement from TAO as input, the reactor antineutrino anomalies will not bias the sub-percent measurement of  $\sin^2 \theta_{13}$ .

### 3.6 The impact of the detector performance

In Sec. 2.1, we assume the energy resolution of the detector to be 10%. The high energy resolution is usually expensive and technically challenging for a large volume liquid scintillator detector. Thus, with the nominal setup, we have a study on the  $\sin^2 \theta_{13}$  precision measurement sensitivity for a detector with different energy resolutions. As shown in Fig. 7, the relative variation of sensitivity would be within 4% for the energy resolution from  $3\%/\sqrt{E(\text{MeV})}$  to  $15\%/\sqrt{E(\text{MeV})}$ . In general, the energy resolution is not a key factor for  $\sin^2 \theta_{13}$  precision measurement at the baseline of  $\sim 2.0$  km. A 10% energy resolution is sufficient for measuring  $\sin^2 \theta_{13}$  to the sub-percent precision level.

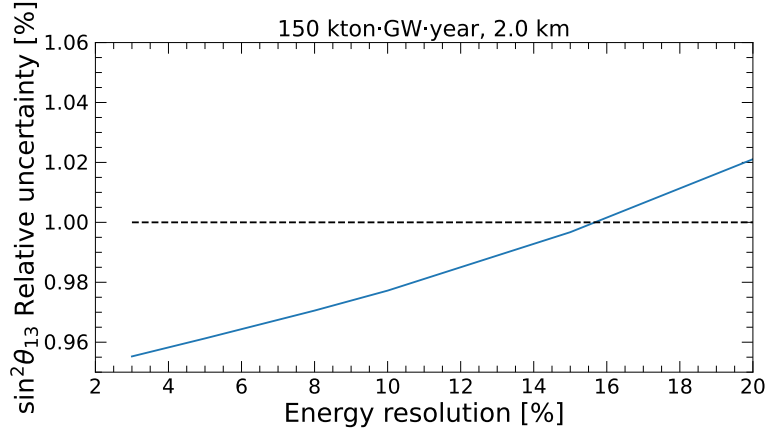


**Figure 7.** The  $\sin^2 \theta_{13}$   $1\sigma$  precision sensitivity for the experiment with different prompt energy resolutions. The  $\sin^2 \theta_{13}$  precision sensitivity relative variation would be within 4% for the energy resolution from  $3\%/\sqrt{E(\text{MeV})}$  to  $15\%/\sqrt{E(\text{MeV})}$ .

As a detector with volume at the kton level, we assume that the energy scale calibration’s high accuracy (uncertainty  $<0.5\%$ ) can be achieved as Daya Bay [39] and JUNO [54]. Nonetheless, even if the energy scale uncertainty is at a 1% level, the  $\sin^2 \theta_{13}$  precision measurement sensitivity keeps almost the same (relative difference  $<0.1\%$ ). The result is consistent with the calibration uncertainty contribution we observe in Fig. 5.

## 4 Conclusion

For measuring  $\sin^2 \theta_{13}$  to the sub-percent level precision, the crucial requirements are the statistics, the baseline, and the control of the spectral shape uncertainty. We perform a numerical calculation of the  $\sin^2 \theta_{13}$  precision measurement sensitivity and find that the optimal baselines for a single liquid scintillator detector setup are different from the identical near and far detectors setup. The latter setup can suppress the rate uncertainties by near-far relative measurement, and the optimal baseline is about 1.8 km. The optimal baseline for the former setup is about 1.3 km at low luminosities  $\lesssim 10 \text{ kton} \cdot \text{GW} \cdot \text{year}$  as the dominant systematics is the rate uncertainty. For larger statistics, as the shape uncertainty becomes dominant, the optimal baseline shifts to about 2.0 km and keeps being so for the integrated luminosity up to  $10^6 \text{ kton} \cdot \text{GW} \cdot \text{year}$ . The reason is that  $\sin^2 \theta_{13}$  characterizes the disappearance amplitude; thus, the rate uncertainty plays an important role in the measurement when the disappearance maximum is at the peak of the unoscillated antineutrino energy spectrum. For a single detector experiment with large rate uncertainty, the optimal baselines shift from the baseline of the maximum rate oscillation.

With the spectral shape uncertainty constrained by the TAO experiment, a single liquid scintillator detector at the baseline of  $\sim 2.0 \text{ km}$  could measure  $\sin^2 \theta_{13}$  to the sub-percent precision level within  $150 \text{ kton} \cdot \text{GW} \cdot \text{year}$  integrated luminosity. The energy resolution is not a key factor for an experiment at several kilometers’ baselines. Thus, we propose to install a single 4 kton, 10% energy resolution detector at  $\sim 2.0 \text{ km}$  from a 17.4 GW reactor



complex like Daya Bay. The experiment with such a setup could measure  $\sin^2 \theta_{13}$  to the sub-percent precision level within three years. Various factors that may increase or decrease the sensitivity are discussed; the dominant factors are the reactor antineutrino spectral shape uncertainty and the  $\sin^2 \theta_{13}$  true value. With the flat relative spectral shape uncertainty given by the nuclear theory community, the optimal baseline is 2.9 km at larger luminosities. The relative shape uncertainty is the same for different energies in this model; thus, the optimal baseline is further shifted to offset the oscillation maximum of 1.8 km at the peak of the reactor neutrino spectrum. The detector performances on the energy resolution and energy scale uncertainty have minor impacts on the sensitivity. The experiment should have good control on the background, including the natural radioactivity and cosmogenic backgrounds, as they may have significant contributions to the shape uncertainty.

## Acknowledgements

This work was supported by the National Key R&D Program of China (2018YFA0404101).

## References

- [1] B. Pontecorvo, *Neutrino Experiments and the Problem of Conservation of Leptonic Charge*, *Zh. Eksp. Teor. Fiz.* **53** (1967) 1717.
- [2] Z. Maki, M. Nakagawa and S. Sakata, *Remarks on the unified model of elementary particles*, *Prog. Theor. Phys.* **28** (1962) 870.
- [3] M.S. Athar et al., *Status and Perspectives of Neutrino Physics*, [2111.07586](#).
- [4] PARTICLE DATA GROUP collaboration, *Review of Particle Physics*, *PTEP* **2020** (2020) [083C01](#).
- [5] JUNO collaboration, *Sub-percent Precision Measurement of Neutrino Oscillation Parameters with JUNO*, [2204.13249](#).
- [6] DAYA BAY collaboration, *Measurement of the Electron Antineutrino Oscillation with 1958 Days of Operation at Daya Bay*, *Phys. Rev. Lett.* **121** (2018) 241805 [[1809.02261](#)].
- [7] DUNE collaboration, *Deep Underground Neutrino Experiment (DUNE), Far Detector Technical Design Report, Volume I Introduction to DUNE*, *JINST* **15** (2020) T08008 [[2002.02967](#)].
- [8] HYPER-KAMIOKANDE collaboration, *Hyper-Kamiokande Design Report*, [1805.04163](#).
- [9] SNO collaboration, *Combined Analysis of all Three Phases of Solar Neutrino Data from the Sudbury Neutrino Observatory*, *Phys. Rev. C* **88** (2013) 025501 [[1109.0763](#)].
- [10] Y. Nakajima, *Recent results and future prospects from super-kamiokande*, in *Presentation at the XXIX International Conference on Neutrino Physics and Astrophysics (Neutrino 2020)*, 2020.
- [11] SUPER-KAMIOKANDE collaboration, *Solar Neutrino Measurements in Super-Kamiokande-IV*, *Phys. Rev. D* **94** (2016) 052010 [[1606.07538](#)].
- [12] KAMLAND collaboration, *Reactor On-Off Antineutrino Measurement with KamLAND*, *Phys. Rev. D* **88** (2013) 033001 [[1303.4667](#)].

- [13] NOVA collaboration, *First Measurement of Neutrino Oscillation Parameters using Neutrinos and Antineutrinos by NOvA*, *Phys. Rev. Lett.* **123** (2019) 151803 [[1906.04907](#)].
- [14] T2K collaboration, *Constraint on the matter–antimatter symmetry-violating phase in neutrino oscillations*, *Nature* **580** (2020) 339 [[1910.03887](#)].
- [15] MINOS collaboration, *Combined analysis of  $\nu_\mu$  disappearance and  $\nu_\mu \rightarrow \nu_e$  appearance in MINOS using accelerator and atmospheric neutrinos*, *Phys. Rev. Lett.* **112** (2014) 191801 [[1403.0867](#)].
- [16] SUPER-KAMIOKANDE collaboration, *Atmospheric neutrino oscillation analysis with external constraints in Super-Kamiokande I-IV*, *Phys. Rev. D* **97** (2018) 072001 [[1710.09126](#)].
- [17] ICECUBE collaboration, *Measurement of Atmospheric Neutrino Oscillations at 6–56 GeV with IceCube DeepCore*, *Phys. Rev. Lett.* **120** (2018) 071801 [[1707.07081](#)].
- [18] RENO collaboration, *Observation of reactor antineutrino disappearance using delayed neutron capture on hydrogen at RENO*, *JHEP* **04** (2020) 029 [[1911.04601](#)].
- [19] DOUBLE CHOOZ collaboration, *Double Chooz  $\theta_{13}$  measurement via total neutron capture detection*, *Nature Phys.* **16** (2020) 558 [[1901.09445](#)].
- [20] NOVA collaboration, *NOvA: Proposal to Build a 30 Kiloton Off-Axis Detector to Study  $\nu_\mu \rightarrow \nu_e$  Oscillations in the NuMI Beamline*, [hep-ex/0503053](#).
- [21] T2K collaboration, *The T2K Experiment*, *Nucl. Instrum. Meth. A* **659** (2011) 106 [[1106.1238](#)].
- [22] JUNO collaboration, *JUNO physics and detector*, *Prog. Part. Nucl. Phys.* **123** (2022) 103927 [[2104.02565](#)].
- [23] L. Wolfenstein, *Neutrino Oscillations in Matter*, *Phys. Rev. D* **17** (1978) 2369.
- [24] S.P. Mikheyev and A.Y. Smirnov, *Resonance Amplification of Oscillations in Matter and Spectroscopy of Solar Neutrinos*, *Sov. J. Nucl. Phys.* **42** (1985) 913.
- [25] E. Lisi and D. Montanino, *Earth regeneration effect in solar neutrino oscillations: An Analytic approach*, *Phys. Rev. D* **56** (1997) 1792 [[hep-ph/9702343](#)].
- [26] E.K. Akhmedov, R. Johansson, M. Lindner, T. Ohlsson and T. Schwetz, *Series expansions for three flavor neutrino oscillation probabilities in matter*, *JHEP* **04** (2004) 078 [[hep-ph/0402175](#)].
- [27] DAYA BAY collaboration, *A side-by-side comparison of Daya Bay antineutrino detectors*, *Nucl. Instrum. Meth. A* **685** (2012) 78 [[1202.6181](#)].
- [28] DAYA BAY collaboration, *Antineutrino energy spectrum unfolding based on the Daya Bay measurement and its applications*, *Chin. Phys. C* **45** (2021) 073001 [[2102.04614](#)].
- [29] V. Kopeikin, L. Mikaelyan and V. Sinev, *Reactor as a source of antineutrinos: Thermal fission energy*, *Phys. Atom. Nucl.* **67** (2004) 1892 [[hep-ph/0410100](#)].
- [30] X.B. Ma, W.L. Zhong, L.Z. Wang, Y.X. Chen and J. Cao, *Improved calculation of the energy release in neutron-induced fission*, *Phys. Rev. C* **88** (2013) 014605 [[1212.6625](#)].
- [31] P. Huber, *On the determination of anti-neutrino spectra from nuclear reactors*, *Phys. Rev. C* **84** (2011) 024617 [[1106.0687](#)].
- [32] T.A. Mueller et al., *Improved Predictions of Reactor Antineutrino Spectra*, *Phys. Rev. C* **83** (2011) 054615 [[1101.2663](#)].

- [33] DAYA BAY collaboration, *Improved Measurement of the Reactor Antineutrino Flux at Daya Bay*, *Phys. Rev. D* **100** (2019) 052004 [[1808.10836](#)].
- [34] RENO collaboration, *Measurement of reactor antineutrino flux and spectrum at RENO*, *Phys. Rev. D* **104** (2021) L111301 [[2010.14989](#)].
- [35] P. Vogel and J.F. Beacom, *Angular distribution of neutron inverse beta decay, anti-neutrino( $e$ ) +  $p \rightarrow e^+ + n$* , *Phys. Rev. D* **60** (1999) 053003 [[hep-ph/9903554](#)].
- [36] A. Strumia and F. Vissani, *Precise quasielastic neutrino/nucleon cross-section*, *Phys. Lett. B* **564** (2003) 42 [[astro-ph/0302055](#)].
- [37] D. Stump, J. Pumplin, R. Brock, D. Casey, J. Huston, J. Kalk et al., *Uncertainties of predictions from parton distribution functions. 1. The Lagrange multiplier method*, *Phys. Rev. D* **65** (2001) 014012 [[hep-ph/0101051](#)].
- [38] DAYA BAY collaboration, *Measurement of electron antineutrino oscillation based on 1230 days of operation of the Daya Bay experiment*, *Phys. Rev. D* **95** (2017) 072006 [[1610.04802](#)].
- [39] DAYA BAY collaboration, *A high precision calibration of the nonlinear energy response at Daya Bay*, *Nucl. Instrum. Meth. A* **940** (2019) 230 [[1902.08241](#)].
- [40] DOUBLE CHOOZ collaboration, *Search for signatures of sterile neutrinos with Double Chooz*, *Eur. Phys. J. C* **81** (2021) 775 [[2009.05515](#)].
- [41] KAMLAND collaboration, *Constraints on  $\theta_{13}$  from A Three-Flavor Oscillation Analysis of Reactor Antineutrinos at KamLAND*, *Phys. Rev. D* **83** (2011) 052002 [[1009.4771](#)].
- [42] JUNO collaboration, *TAO Conceptual Design Report: A Precision Measurement of the Reactor Antineutrino Spectrum with Sub-percent Energy Resolution*, [2005.08745](#).
- [43] M. Estienne et al., *Updated Summation Model: An Improved Agreement with the Daya Bay Antineutrino Fluxes*, *Phys. Rev. Lett.* **123** (2019) 022502 [[1904.09358](#)].
- [44] A.C. Hayes, J.L. Friar, G.T. Garvey, D. Ibeling, G. Jungman, T. Kawano et al., *Possible origins and implications of the shoulder in reactor neutrino spectra*, *Phys. Rev. D* **92** (2015) 033015 [[1506.00583](#)].
- [45] DAYA BAY collaboration, *Improved Measurement of the Reactor Antineutrino Flux and Spectrum at Daya Bay*, *Chin. Phys. C* **41** (2017) 013002 [[1607.05378](#)].
- [46] JUNO collaboration, *Radioactivity control strategy for the JUNO detector*, *JHEP* **11** (2021) 102 [[2107.03669](#)].
- [47] KAMLAND collaboration, *Production of Radioactive Isotopes through Cosmic Muon Spallation in KamLAND*, *Phys. Rev. C* **81** (2010) 025807 [[0907.0066](#)].
- [48] BOREXINO collaboration, *Comprehensive geoneutrino analysis with Borexino*, *Phys. Rev. D* **101** (2020) 012009 [[1909.02257](#)].
- [49] DAYA BAY collaboration, *Observation of electron-antineutrino disappearance at Daya Bay*, *Phys. Rev. Lett.* **108** (2012) 171803 [[1203.1669](#)].
- [50] P. Huber, M. Lindner, T. Schwetz and W. Winter, *Reactor neutrino experiments compared to superbeams*, *Nucl. Phys. B* **665** (2003) 487 [[hep-ph/0303232](#)].
- [51] M.C. Gonzalez-Garcia, M. Maltoni and T. Schwetz, *NuFIT: Three-Flavour Global Analyses of Neutrino Oscillation Experiments*, *Universe* **7** (2021) 459 [[2111.03086](#)].

- [52] F. Capozzi, E. Di Valentino, E. Lisi, A. Marrone, A. Melchiorri and A. Palazzo, *Unfinished fabric of the three neutrino paradigm*, *Phys. Rev. D* **104** (2021) 083031 [[2107.00532](#)].
- [53] P.F. de Salas, D.V. Forero, S. Gariazzo, P. Martínez-Miravé, O. Mena, C.A. Ternes et al., *2020 global reassessment of the neutrino oscillation picture*, *JHEP* **02** (2021) 071 [[2006.11237](#)].
- [54] JUNO collaboration, *Calibration Strategy of the JUNO Experiment*, *JHEP* **03** (2021) 004 [[2011.06405](#)].